

Relaxometric and Modelling Studies of the Binding of a Lipophilic Gd-AAZTA Complex to Fatted and Defatted Human Serum Albumin

Eliana Gianolio,^[a] Giovanni B. Giovenzana,^[b] Dario Longo,^[a] Irene Longo,^[a] Ivan Menegotto,^[b] and Silvio Aime*^[a]

Abstract: A new lipophilic gadolinium chelate consisting of a long aliphatic chain bound to the AAZTA coordination cage (Gd-AAZTAC17) has been synthesised. It possesses two coordinated water molecules ($q=2$) in fast exchange with the solvent ($\tau_M^{298}=67$ ns), which yields a relaxivity of $10.2 \text{ mM}^{-1}\text{s}^{-1}$. At concentrations greater than 0.1 mM , it forms micelles (average diameter 5.5 nm) characterised by a relaxivity of approximately $30 \text{ mM}^{-1}\text{s}^{-1}$ at 20 MHz and 298 K . The latter value appears to be “quenched” by magnetic interactions among the Gd^{III} ions on the surface of the micelle that cause a decrease in the electronic relaxation time. A relaxivity of

$41 \text{ mM}^{-1}\text{s}^{-1}$ was recorded for this micellar system when 98% of the Gd^{III} ions were replaced by diamagnetic Y^{III} . Gd-AAZTAC17 exhibits a better affinity for fatted human serum albumin (HSA) than for defatted HSA, whereas the relaxivities of the supramolecular adducts are reversed. The relaxivity shown by Gd-AAZTAC17/defatted HSA (r_1^{H} (20 MHz , 298 K) = $84 \text{ mM}^{-1}\text{s}^{-1}$) is by far the highest relaxivity reported so far for non-covalent paramagnetic adducts with slow-moving substrates.

Keywords: albumin • contrast agents • gadolinium • magnetic resonance imaging • micelles

As shown by molecular docking calculations, the gadolinium complex enters a hydrophobic pocket present in fatted HSA more extensively than the corresponding adduct with defatted HSA. Interestingly, no marked difference was observed in either the relaxation enhancement or the binding affinity between fatted and defatted HSA when the binding titrations were carried out at a Gd-AAZTAC17 concentration higher than its critical micellar concentration (cmc). This behaviour has been attributed to the formation of an association between the negatively charged micelle of the lipophilic metal complexes and the positive residues on the surface of the protein.

Introduction

It is now well established that the information content of a magnetic resonance imaging (MRI) experiment can be significantly enhanced by the use of a suitable contrast agent (CA). Nowadays about 35% of MRI scans make use of

CAs and it is expected that this percentage will further increase with the availability of more sensitive and specific agents.^[1–4] A MRI CA is not directly visualised in the image, only its effects on water proton relaxation times are observed. The increased relaxation rates allow the attainment of an intense signal in a short time and a better signal-to-noise ratio by the acquisition of a higher number of measurements.

As unpaired electrons display a remarkable ability to reduce T_1 and T_2 , the search for efficient CAs has focussed on paramagnetic metal complexes. The metal of choice has been the Gd^{III} ion for its high paramagnetism (seven unpaired electrons) and for its favourable properties in terms of electronic relaxation.^[5] This ion forms very stable complexes with polyamminocarboxylate ligands and Gd-DTPA (Magnevist) was the first MRI CA approved for clinical use. Since then, other Gd^{III} -based CAs similar to Magnevist have been introduced into clinical practice. They have very similar pharmacokinetic properties because they are distributed in the extracellular fluid and are eliminated via glomerular

[a] Dr. E. Gianolio, Dr. D. Longo, Dr. I. Longo, Prof. S. Aime
Dipartimento di Chimica I.F.M. e
Centro di eccellenza per l'Imaging Molecolare
Università degli Studi di Torino
Via P. Giuria 7, 10125 Torino (Italy)
Fax: (+39)116-707-855
E-mail: silvio.aime@unito.it

[b] Prof. G. B. Giovenzana, Dr. I. Menegotto
Dipartimento di Scienze Chimiche Alimentari, Farmaceutiche e
Farmacologiche
Università del Piemonte Orientale “A. Avogadro”
Via Bovio 6, 28100 Novara, (Italy)

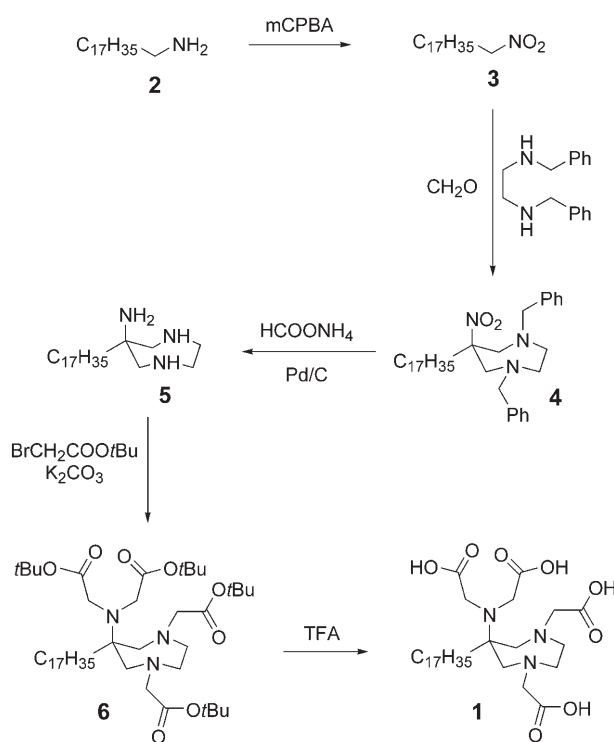
Supporting information for this article is available on the WWW under <http://www.chemeurj.org> or from the author.

filtration. The relative ability of a paramagnetic metal complex to act as a MRI CA is expressed by its relaxivity, that is, the property that is a measure of the relaxation enhancement of water protons in solution containing the paramagnetic agent at a 1 mM concentration.^[6] Much work has been carried out in the last two decades to improve the relaxivity of Gd^{III}-based agents. It was recognised early on that high relaxivities can be attained for slow-moving systems endowed with fast exchange rates of the coordinated water molecule(s) and suitably long electronic relaxation rates of the unpaired electrons on the metal ion.^[3,4,7] On this basis several macromolecular systems have been designed in which the Gd^{III} chelates are either covalently or non-covalently bound to high molecular weight substrates. In particular much attention has been devoted to supramolecular adducts formed by suitably functionalised Gd^{III} chelates and human serum albumin (HSA).^[8] Although the theory of paramagnetic relaxation foresees for the latter systems r_1 values of the order of $100 \text{ mM}^{-1} \text{ s}^{-1}$ (at the observation frequency of 20 MHz), the relaxivities of the numerous reported systems have never reached such high values. The highest reported r_1 value ($65.8 \text{ mM}^{-1} \text{ s}^{-1}$)^[9] is relative to the adduct of HSA with a Gd-TTDA-BOM derivative. Often low r_1 values have been ascribed to an insufficiently fast exchange of the coordinated water molecules^[10] and this drawback has generated a number of studies aimed at the understanding of the relationships between the structure of the chelate and the lifetime of the coordinated water. In this context, it has been suggested that the problems in attaining the theoretically expected relaxivities might also be due to the inner rotation of the water molecule around its axis of coordination to the metal ion.^[11,12] Such local motion superimposed on the overall molecular tumbling quenches the relaxation enhancement expected for slow-moving macromolecular systems. If this is the case, the high relaxivity target has to be pursued by exploring other routes. For instance, by increasing the number of water molecules coordinated to the Gd^{III} ion as relaxivity increases with the hydration state. An increase in the number of coordinated water molecules can be obtained by reducing the denticity of the ligand and this often occurs at the expense of the overall thermodynamic stability which is one of the primary requisites of a Gd^{III} complex for it to be considered as a potential CA for in vivo investigations. In this context the first system to be investigated was Gd-DO3A, but it was soon realised that, in a biological fluid, its coordinated water molecules are replaced by endogenous ions like lactate and carbonate.^[13,14] A related system is represented by Gd-PCTA whose coordinated water molecules are not so easily replaced by endogenous ligands.^[15-17] However, its further functionalisation for binding to a macromolecular substrate proved to be rather difficult. In addition to polyaminocarboxylate ligands, there is the interesting class of HOPO ligands developed by Raymond and co-workers.^[18-20] Their complexes with Gd^{III} are outstandingly stable and their potential for MRI applications appears very good. Recently we reported a new heptadentate ligand, namely AAZTA,^[21] characterised by several properties favourable

for use as a MRI CA. Herein we report on our studies on a lipophilic Gd-AAZTA-based system aimed at assessing the relaxation enhancement capabilities of slow-moving paramagnetic adducts formed by its self-assembly and its binding to HSA.

Results and Discussion

Synthesis: The synthesis of AAZTAC17 is analogous to that reported for the parent AAZTA ligand.^[21] Therefore it is simple and relies on readily available and cheap chemicals. First 1-nitrooctadecane was synthesised by oxidation of octadecanamine with *m*-chloroperoxybenzoic acid (*m*CPBA) in refluxing 1,2-dichloroethane (Scheme 1). The aliphatic ni-



Scheme 1. Scheme of the synthesis of AAZTAC17 ligand

troalkane was then employed in the key step involving the formation of the seven-membered ring through the high-performing double nitro-Mannich reaction with *N,N'*-dibenzylethylenediamine and paraformaldehyde. Catalytic transfer hydrogenation of the nitro group and combined hydrogenolysis of the *N*-benzyl groups was achieved with ammonium formate and Pd/C. The triamine was then alkylated by reaction with *tert*-butyl bromoacetate. Finally the *tert*-butyl esters were removed in neat TFA to give the desired ligand.

As for the parent AAZTA ligand, the gadolinium complex of AAZTAC17 is prepared by simply stirring stoichiometric amounts of the ligand and GdCl₃ at neutral pH at ambient temperature.

Relaxometric characterisation: The presence of the aliphatic chain is responsible for the concentration effects on the relaxation enhancement properties of Gd-AAZTAC17. In fact, functionalisation of the AAZTA ligand with the C17 moiety induces the formation of micelles already at submillimolar concentrations. The critical micellar concentration (cmc) of the system was conveniently determined by measuring the ^1H relaxation rates as a function of Gd^{III} complex concentration (Figure 1).

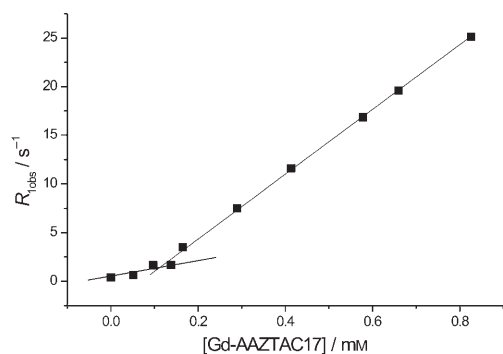


Figure 1. Plot of the variation of the observed longitudinal proton relaxation rate as a function of the concentration of Gd-AAZTAC17 at 0.47 T and 25 °C.

In general, titration of a ligand solution with Gd^{III} ions leads to the formation of a paramagnetic complex and a straight line for the relaxivity versus Gd^{III} complex concentration plot is obtained [Eq. (1)] whose slope corresponds to the relaxivity (r_{1p}) of the complex, where R_{1w} is the diamagnetic contribution of pure water (0.38 s^{-1}).^[22]

$$R_{\text{obs}} = [\text{Gd-L}]r_{1p} + R_{1w} \quad (1)$$

In the case of a self-assembling system such as Gd-AAZTAC17, sharp variation of the linear slope is observed when the system passes from the monomeric state to micellar aggregates. From the data reported in Figure 1, a cmc value of 0.108 mM was determined.

At 20 MHz and 298 K, the relaxivity of Gd-AAZTAC17 below the cmc is $10.2 \text{ mM}^{-1} \text{ s}^{-1}$, whereas the relaxivity of the self-assembled complex above the cmc is $30.0 \text{ mM}^{-1} \text{ s}^{-1}$. The relaxivity of the non-associated form is around 30% higher than that of the parent Gd-AAZTA which is fully consistent with the increase in molecular weight caused by the introduction of the long aliphatic chain.

From an analysis of the temperature dependence of the transverse relaxation rate of the metal-bound ^{17}O water resonance^[23,24] (Figure 2) we obtained a τ_{M}^{298} value of 67 ns for Gd-AAZTAC17 above the micellar concentration, a value that is even smaller than that reported for the parent complex Gd-AAZTA (90 ns)^[21] and so is in the optimal range for the attainment of high relaxivities in the presence of long molecular reorientational times.

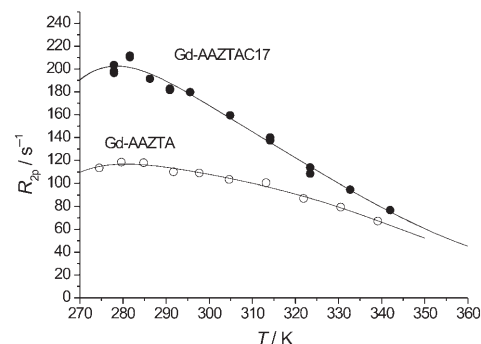


Figure 2. Temperature dependence of the transverse ^{17}O water relaxation rate (R_{2p}) for a 7 mM solution of Gd-AAZTAC17 (●) and Gd-AAZTA (○) at 2.1 T and neutral pH.

At the field used for the relaxometric experiments (0.47 T), the ^1H relaxivity of Gd^{III} complexes is given by Equation (2), where K is a constant related to the strength of the dipolar interaction between the protons and the electronic magnetic moment and τ_{R} is the correlation time associated with the reorientation of the Gd–H magnetic vector.

$$r_{1p} \propto \frac{1}{T_{1M}^{\text{H}}} = Kf(\tau_{\text{R}}) \quad (2)$$

The effect of aggregation may be estimated by analysing the profile of the relaxivity data as a function of the applied field strength. In fact from a quantitative analysis of the NMRD (nuclear magnetic relaxation dispersion)^[22] profiles it is possible to determine the reorientational correlation time (τ_{R}) which is related to the size of the investigated system. The NMRD profiles of Gd-AAZTAC17 at 25 and 37 °C are reported in Figure 3. For the micellar system, data were analysed using the Solomon–Bloembergen–Morgan model modified according to the Lipari–Szabo approach (see Supporting Information). This approach distinguishes between two independent motions: a rapid local motion governed by a correlation time defined as τ_1 and a slower

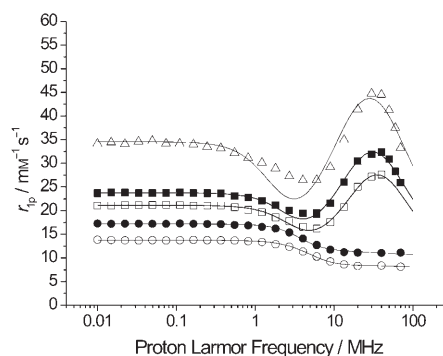


Figure 3. $1/T_1$ NMRD profiles of a 1 mM solution of Gd-AAZTAC17 micelles measured at 25 (■) and 37 °C (□), of the Gd-AAZTAC17 monomer measured at 25 (●) and 37 °C (○) and of Gd-Y-AAZTAC17 micelles at 25 °C (△). The solid curves through the data points were calculated using the parameters reported in Table 2.

Table 1. Principal relaxometric parameters for the different Gd-AAZTAC17-containing systems determined by NMRD and 17O-R_{2p} -VT analysis.

	r_{1p} (20 MHz) [$\text{mM}^{-1}\text{s}^{-1}$]	Δ^2 [s^{-2}]	τ_v [ps]	τ_1 [ps]	τ_g [ps]	S	τ_M [ns]	q
Gd-AAZTAC17 micelles 25°C	30.0	$1.43 \pm 0.28 \times 10^{19}$	43 ± 3.1	295 ± 60	2540 ± 130	0.40 ± 0.15	67 ± 19	2 ^[a]
Gd-AAZTAC17 micelles 37°C	25.0	$1.83 \pm 0.13 \times 10^{19}$	37 ± 1.2	222 ± 30	2338 ± 255	0.40 ± 0.14	29 ± 7.1	2 ^[a]
Gd-YAAZ-TAC17 micelles 25°C	41.4	$9.53 \pm 3.5 \times 10^{18}$	42 ± 5.3	474 ± 75	2530 ± 350	0.48 ± 0.16	67 ^[a]	2 ^[a]
Gd-AAZTAC17 monomer 25°C	10.2	$1.51 \pm 0.1 \times 10^{19}$	35 ± 1.3		142 ± 1.6	–	–	2 ^[a]
Gd-AAZTAC17 monomer 37°C	7.35	$3.87 \pm 0.14 \times 10^{19}$	23 ± 0.75		100 ± 1.15	–	–	2 ^[a]

[a] These parameters were fixed during the fitting procedure.

global motion with a correlation time defined as τ_g . Data resulting from the fitting of the NMRD profiles are reported in Table 1 and are in accordance with other similar micellar systems.^[25,26] Clearly micellisation of the C17 complex gives rise to a system with a slower molecular tumbling relative to the monomeric complex, but the resulting relaxivity appears still lower than the expected values as internal motions are faster than the overall tumbling of the micellar system. Recently Merbach and co-workers demonstrated that interactions between nearby paramagnetic centres in micellar systems increase the transverse electronic relaxation of the electron spins of Gd^{III} and, therefore, reduce the attainable water proton relaxivity.^[27] This drawback may be removed by diluting the Gd^{III} ions with diamagnetic Y^{III} ions in order to increase the average distance between neighbouring Gd^{III} ions. The NMRD profile of mixed micelles formed with 2% Gd^{III} and 98% Y^{III} at the same temperature and pH is reported in Figure 3 (Δ). An enhancement in the relaxivity of around 40% over all the frequency range was observed.

The effect of replacing gadolinium with yttrium is two-fold, namely, 1) it lengthens the electronic relaxation time (and this mainly affects r_{1p} values at low magnetic fields) and 2) it gives rise to a change in the reorientational time that causes an increase in r_{1p} at high magnetic fields. The latter effect appears to be associated with an anisotropic tumbling of the yttrium/gadolinium mixed micelles with the gadolinium-containing monomers aligned along the main rotational axis.

The relaxivity of Gd-AAZTA is constant in the pH range 4–12 (Figure 4), suggesting an overall stability of the complex in this pH range. Progressive protonation of the carboxylic groups at pH values of less than 4 causes the neutralisation of the system and the consequent formation of a precipitate. At basic pH, in contrast to what is reported for other $q=2$ gadolinium complexes such as Gd-DO3A ,^[11] the relaxivity remains constant, suggesting nearly complete inertness

towards the interaction with bicarbonate and hydroxide anions present in solution.

Assessment of micellar size and aggregation number (N_{agg}): Size measurements were performed using a dynamic light scattering instrument (DLS) (also known as photon correlation spectroscopy), which measures Brownian motion in solution and relates them to the sizes of the particles. The method involves illuminating the particles with a laser and analysing the intensity fluctuations in the scattered light. Particles suspended in a liquid are never stationary as

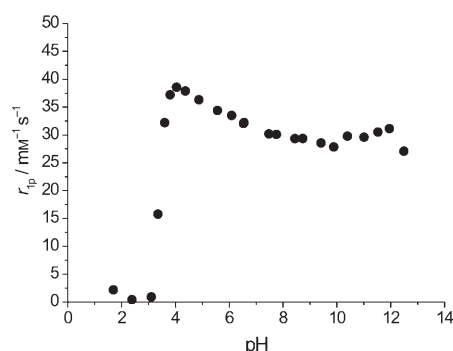


Figure 4. pH dependence of the proton relaxivity (r_{1p}) of Gd-AAZTAC17 micelles measured at 0.47 T and 25°C.

they are constantly moving as a result of Brownian motion. The relationship between the size of a particle and its speed due to Brownian motion is defined by the Stokes–Einstein equation.

A correlator, within the instrument, measures the degree of similarity between two signals recorded in the same position over a period of time. As particles move within the sample, therefore, the correlation decreases with time. A perfect correlation is reported as 1 and no correlation is reported as 0. Correlation functions for large and small particles will therefore be different as the rate of decay is much faster for small particles than it is for large ones. After the correlation function has been measured this information can then be used to calculate the size distribution.

Measurements were taken at room temperature on solutions of Gd-AAZTAC17 at different concentrations above the cmc. The size distribution diagram showed that one main species is present that has a mean diameter of (5.5 ± 0.15) nm (see the Supporting Information).

As static light scattering (SLS) is a valid method^[28–31] for determining the apparent weight-average molar mass of a

solute (M_{app}), the aggregation number (N_{agg}) of Gd-AAZTAC17 micelles has been calculated by dividing M_{app} by the molecular weight of Gd-AAZTAC17.

The Rayleigh expression describing the intensity of light scattered by a particle in solution is given by Equation (3), where K is an optical constant defined in Equation (4), C is the particle concentration, R_{θ} is the Rayleigh ratio of scattered to incident light intensity, M is the average molecular weight, A_2 is the second virial coefficient, $1/P_{\theta}$ is an angle-dependent term defined in Equation (5), λ_0 is the wavelength of the incident light in a vacuum, N_A is Avogadro's number, n_0 is the solvent refractive index, dn/dc is the solvent and analyte-dependent refractive index increment, R_g is the radius of gyration and θ is the scattering angle.

$$\frac{KC}{R_{\theta}} = \left(\frac{1}{M} + 2A_2C \right) \frac{1}{P_{\theta}} \quad (3)$$

$$K = \frac{2\pi^2}{\lambda_0^4 N_A} \left(n_0 \frac{dn}{dc} \right)^2 \quad (4)$$

$$\frac{1}{P_{\theta}} = 1 + \frac{16\pi^2 n_0^2 R_g^2}{3\lambda_0^2} \sin^2 \left(\frac{\theta}{2} \right) \quad (5)$$

The Rayleigh ratio (R_{θ}) term in Equation (3) is the ratio of the scattered to incident light intensity. As the intensity of incident light interacting with a molecule is difficult to measure, the standard approach is to measure the scattering intensity of the analyte relative to that of a well-described standard with a known Rayleigh ratio. A common standard used in light scattering is toluene. The expression used to calculate the sample Rayleigh ratio from a toluene standard is given in Equation (6), where I_A is the residual scattering intensity of the analyte (sample intensity-solvent intensity), I_T is the toluene scattering intensity, n_0 is the solvent refractive index, n_T is the toluene refractive index and R_T is the toluene Rayleigh ratio.

$$R_{\theta} = \frac{I_A n_0^2}{I_T n_T^2} R_T \quad (6)$$

The $1/P_{\theta}$ term in Equation (5) embodies the angular dependence of the sample scattering intensity. The angular dependence arises from different points within a particle or molecule. This phenomenon is known as Mie scattering. When the particles in solution are much smaller than the wavelength of the incident light (for particles with hydrodynamic diameter < 80 nm the molecular weight errors are $< 5\%$),^[32] Mie scattering is minimised and $1/P_{\theta}$ reduces to 1.

So, for pure Rayleigh scattering, Equation (3) can be reduced to Equation (7) such that a plot of KC/R_{θ} versus C (Debye plot) is expected to be linear with an intercept equivalent to $1/M$.

$$\frac{KC}{R_{\theta}} = \frac{1}{M} + 2A_2C \quad (7)$$

Fitting of experimental data (see the Supporting Information) gave an apparent molecular weight of (70.9 ± 1.203) kDa. From the ratio of this value to the molecular weight of Gd-AAZTAC17, an N_{agg} (aggregation number) value of 95 was determined.

Binding to HSA: Owing to the possible angiographic MRI applications for this system, the interaction with human serum albumin has been investigated in detail both in the case of the monomeric gadolinium complex (below the cmc) and in the case of the aggregated micellar system (above the cmc).

The binding of Gd-AAZTAC17 to HSA below the critical micellar concentration was conveniently assessed by measuring the water proton relaxation rates of solutions containing the paramagnetic complex and increasing concentrations of the serum protein (PRE method).^[10] In addition to yielding an estimate of the binding strength (nK_A , where n is the number of binding sites) these measurements also provide a direct assessment of the relaxivity of the macromolecular adduct (r_1^b).

Analysis of the relaxometric data obtained from the titration of a $20 \mu\text{M}$ aqueous solution of the Gd^{III} complex with fatted and defatted HSA at pH 7.4 and 298 K (Figure 5) al-

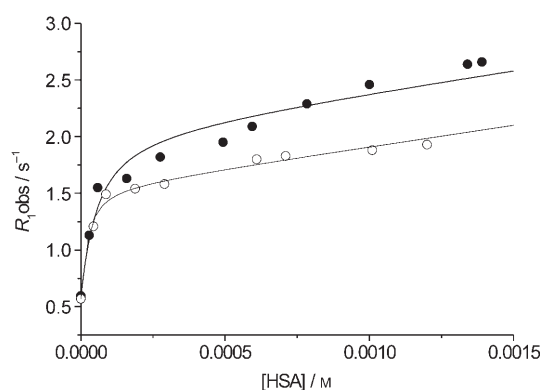


Figure 5. Plot of the variation of the observed longitudinal water proton relaxation rate of a $20 \mu\text{M}$ solution of Gd-AAZTAC17 as a function of fatted (\circ) and defatted (\bullet) HSA concentration (0.47 T, 25°C).

lowed us to determine the nK_A and r_1^b values reported in Table 2. The binding affinity increases significantly on going from defatted to fatted HSA, whereas the relaxivity of the paramagnetic macromolecular adduct is markedly higher for defatted HSA. Binding of this lipophilic gadolinium complex to defatted HSA leads to the highest relaxivity ever reported for a stable gadolinium chelate bound to a slow-moving substrate. The value of $84 \text{ mM}^{-1} \text{ s}^{-1}$ (at 20 MHz) is 30% larger than the most efficient system reported until now.

Although it has been possible to identify the domain of the interaction of Gd-AAZTAC17 with HSA on the basis of competition assays with palmitic acid, warfarin and ibupro-

Table 2. Binding parameters for Gd-AAZTAC17 (as a monomer and as micelles) and Gd-Y-AAZTAC17 systems determined using the PRE method at 25 °C in phosphate buffer solutions.

		Defatted HSA	Fatted HSA
Gd-AAZTAC17 (under cmc)	nK_A [$10^4 M^{-1}$]	2.3 ± 0.7	7.1 ± 1.8
	r_1^b [$mm^{-1} s^{-1}$]	84 ± 3.3	63 ± 1.3
Gd-AAZTAC17 (above cmc)	nK_A [$10^5 M^{-1}$]	1.5 ± 0.4	1.7 ± 0.6
	r_1^b [$mm^{-1} s^{-1}$]	36.8 ± 0.34	35.5 ± 0.21
Gd/Y-AAZTAC17 (above cmc)	nK_A [$10^5 M^{-1}$]	1.1 ± 0.26	–
	r_1^b [$mm^{-1} s^{-1}$]	42.3 ± 0.45	–

fen, access to details of the binding mode has only become possible thanks to molecular docking studies (see below).

The binding of fatty acids to serum albumin has been studied for over 40 years, but a complete understanding of the determinants of these interactions has not yet been reached. Although it is now well established that the protein has multiple fatty acid binding sites of different affinity,^[33–35] the precise number of binding sites is not known. The current consensus seems to be that there are two or three high affinity sites and at least three further sites of lower affinity.^[34,35] In particular, two of these lower-affinity binding sites (named as sites 6 and 7) seem to be the favourite ones for the binding of the complex under scrutiny. These two sites are located on albumin in the region of subdomain IIA^[33–38] (corresponding to Sudlow's site I).

Upon addition of three equivalents of palmitic acid to the defatted HSA the resulting relaxivity of the supramolecular adduct with Gd-AAZTAC17 is the same as that found for the fatted HSA-containing system. Furthermore, addition of palmitic acid to the solution containing the fatted HSA/Gd-AAZTAC17 adduct leads to a progressive decrease in the observed relaxivity (Figure 6).

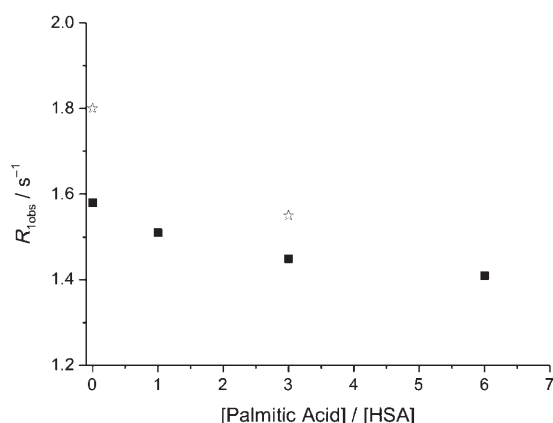


Figure 6. Plot of the variation of the observed longitudinal water proton relaxation rate of Gd-AAZTAC17 bound to fatted (■) and defatted (☆) HSA as a function of increasing concentration of palmitic Acid (0.47 T, 25 °C).

Further insights into the identification of the binding site were obtained by carrying out a competitive assay with warfarin, a well-established ligand for binding to HSA Sudlow's site I.^[39] As shown in Figure 7, warfarin removes the gadolinium complex with either fatted and defatted HSA although the r_1 decrease is slower in the case of fatted HSA, as was expected on the basis of the higher affinity shown by Gd-AAZTAC17 for this form. The addition of the same amounts of ibuprofen, a classical competitor for Sudlow's site II, to the adducts of Gd-AAZTAC17 with fatted and defatted HSA showed no competition effect.

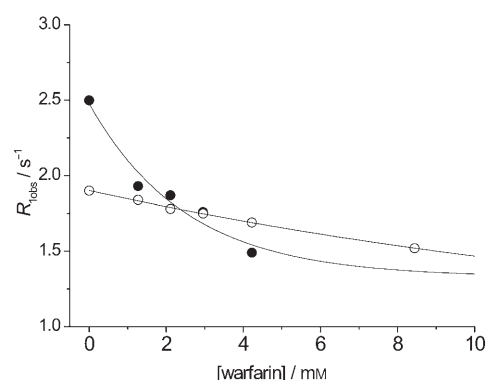


Figure 7. Plot of the variation of the observed longitudinal water proton relaxation rate of Gd-AAZTAC17 bound to fatted (○) and defatted (●) HSA as a function of increasing concentration of warfarin (0.47 T, 25 °C).

Furthermore, it is known that, at low concentrations,^[40,41] the presence of long-chain fatty acids such as palmitic acid (C16) actually enhances the binding of warfarin and other site I binding molecules (i.e., bilirubin and triiodobenzoic acid); at high molar ratios long-chain fatty acids start to displace the drug.^[42] The K_a values obtained for the compound under study towards fatted and defatted HSA suggest that similar behaviour may also occur in the binding of Gd-AAZTAC17; in fact, in the case of fatted HSA (2–3 equivalents of fatty acid are normally bound to human albumin in serum), the observed affinity is higher than with defatted HSA.

Allosteric effects related to the presence of fatty acids on the protein are due to the dramatic conformational changes they induce in the protein structure;^[43,44] the rotations of the three domains of the protein cause the opening of the central cervix with the width of the molecule increasing from 80 to 90 Å. These conformational changes are responsible for the difference in the binding affinity of Gd-AAZTAC17 with fatted and defatted HSA.

The NMRD profiles of the adducts of Gd-AAZTAC17 with fatted and defatted HSA have been recorded in the range of 0.01–70 MHz at 25 °C in phosphate buffer (Figure 7).

The experimental data reported in Figure 8 can be analysed only qualitatively as the investigated system appears to be too complex for quantitative fitting. Both profiles display a high relaxivity peak centred at around 30 MHz, typi-

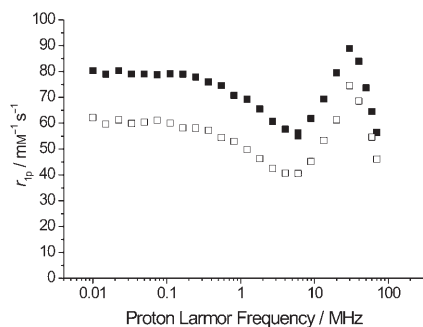


Figure 8. $1/T_1$ NMRD profiles of a 1 mM solution of Gd-AAZTAC17 bound to defatted (■) and fatted (□) HSA.

cal of systems endowed with long τ_r values. As both systems also exhibit quite high relaxivities in the low frequency range, the observed profiles suggest a large contribution to the relaxivity arising from water protons in the second coordination sphere of the chelate.

This contribution may be regarded as originating from clusters of water molecules grafted in the proximity of the chelate core just outside the hydrophobic pocket in which the aliphatic chain is inserted. Analogous second-coordination-sphere contributions were previously reported for the adducts formed upon non-covalent binding of a paramagnetic complex at the surface of a protein^[8] as well as in the supramolecular “host-guest” adduct formed by poly- β -cyclodextrin and Gd^{III} complexes.^[44]

As confirmed by molecular docking studies on the accessible solvent surface (see below), the difference in the relaxivities of fatted and defatted HSA adducts can be mainly ascribed to changes in the contribution of the second hydration sphere. Further support for the large contribution to the relaxivity arising from the second hydration shell of the complex bound to HSA comes from the variation of the longitudinal proton relaxation rates as a function of temperature. Values of r_1^b (at 20 MHz) versus temperature are reported in Figure 9. Experimental data may be interpolated

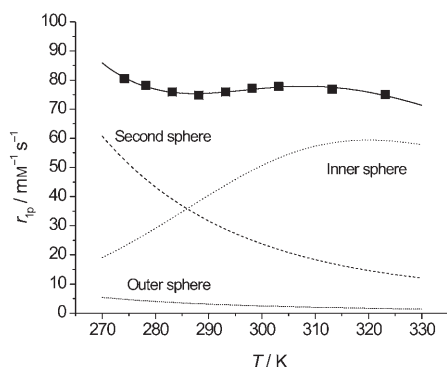


Figure 9. Temperature dependence of the water proton relaxivity of the Gd-AAZTAC17/defatted HSA adduct (0.47 T). The calculated contributions from water molecules in the inner, second and outer coordination spheres to the observed relaxivity of the Gd-AAZTAC17/defatted HSA supramolecular adduct are also reported.

using a model that provides contributions from inner, second and outer coordination spheres. As shown in the graphical separation of these three contributions, the decrease in relaxivity in the first part of the curve (low temperatures) is due to the large second-sphere contribution, whereas the bell-shaped second part is essentially associated with the inner-sphere contribution, which, in turn, seems to be determined by a relatively long coordinated water exchange lifetime. Interestingly, the concomitant effect of a high τ_M value for coordinated water molecules and the large second-coordination-sphere contribution makes the overall relaxivity of the Gd-AAZTAC17/defatted HSA adduct almost independent of temperature.

Gd-AAZTAC17 micelle/HSA supramolecular adduct: Binding to HSA has also been investigated for concentrations of Gd-AAZTAC17 well above the critical micellar concentration (e.g., 1.3 mM for the titration reported in Figure 10). In-

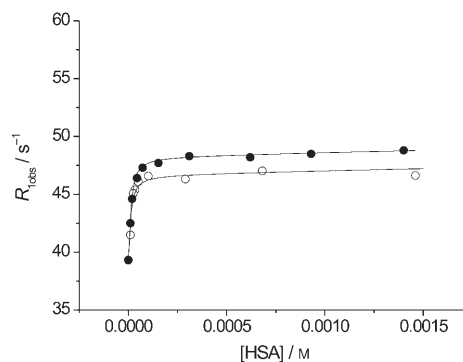


Figure 10. Plot of the variation of the observed longitudinal water proton relaxation rate of a 1.3 mM solution of Gd-AAZTAC17 as a function of fatted (○) and defatted (●) HSA concentration (0.47 T, 25 °C).

terestingly, the behaviour shown by the micellar system was quite different to the one observed when Gd-AAZTAC17 binds to HSA as a monomeric species.

Besides a slight increase in the relaxivity of the bound form with respect to the free micellar system, very similar values for the relaxivity of the bound forms were observed with fatted and defatted HSA. This suggests that, above the cmc, a supramolecular adduct is formed between the pre-formed micelle and HSA. Such an association appears to be driven by electrostatic interactions among the negative charges of the micelles and the positively charged residues exposed on the surface of the protein (Figure 11). In fact, the increase in the ionic strength of the solution upon addition of NaCl invariably caused a decrease in the observed water proton relaxation rates.

Clearly, when the Gd-AAZTAC17 micelle is electrostatically bound to HSA, any conformational change in the structure of albumin brought about by the binding of fatty acids does not interfere with the binding determinants that are represented by positively charged amino acid residues.

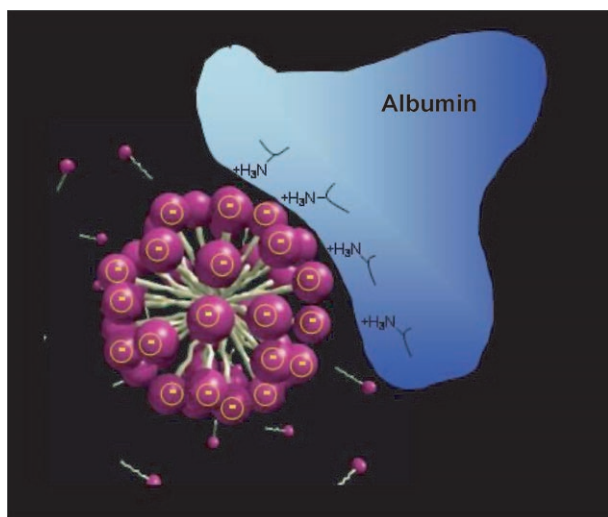


Figure 11. Schematic representation of the electrostatic interaction between the Gd-AAZTAC17 micelle and HSA.

As each micelle is formed by about 95 Gd-AAZTAC17 units, K_A values of 1.5×10^5 and $1.7 \times 10^5 \text{ M}^{-1}$ have been estimated for the interaction of the micelle with defatted and fatted HSA, respectively.

Further support for the supramolecular assembly formed by the micelle and HSA has been gained by determining the adduct size by the dynamic light scattering technique. The mean diameter measured for the adduct (1:1 HSA/micelle) was 11.5 nm, which nicely corresponds to the sum of the size of albumin (experimental mean diameter ca. 6 nm) and the size of the micelles (ca. 5.5 nm) (Figure 12).

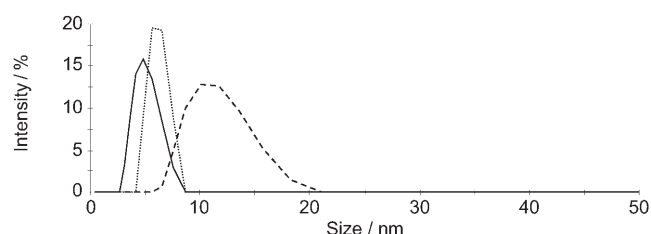


Figure 12. Comparative size distribution diagram, measured by dynamic light scattering, of three independent solutions containing a) the Gd-AAZTAC17 micelle ($[\text{Gd}] = 0.55 \text{ mM}$) (—), b) HSA ($[\text{HSA}] = 0.0055 \text{ mM}$) (.....) and c) the Gd-AAZTAC17 micelle/HSA adduct ($[\text{Gd}] = 0.55 \text{ mM}$, $[\text{HSA}] = 0.0055 \text{ mM}$) (-----).

It is reasonable to surmise that the formation of the micelle/HSA assembly is accompanied by the translocation of Gd-AAZTAC17 monomers to the protein binding sites, as described above. Therefore the observed relaxivity, though mainly determined by gadolinium chelates organised in the micellar form, also contains a contribution from the Gd-AAZTAC17/HSA adduct. This may account for the slightly higher relaxivity observed for the defatted HSA system (Figure 10).

Further support for this view was obtained by using the above described micelles formed with 98% Y-AAZTAC17

and 2% Gd-AAZTAC17. Now the increase in relaxivity brought about by this system (compared with the “all-Gd” system) is only a few percentage units because the translocation to the protein of diamagnetic Y-AAZTAC17 units rules out the contribution arising from the paramagnetic adduct with HSA. Thus the observed relaxation enhancement observed with Gd/Y mixed micelles comes only from the factors described above.

Molecular docking studies for the characterisation of the binding site: In order to gain more insight into the differences in the binding mode of Gd-AAZTAC17 to fatted and defatted HSA we carried out a molecular docking investigation. The competitive assays described above with palmitic acid and warfarin clearly indicate that the binding region of Gd-AAZTAC17 is represented by Sudlow’s site I.

Moreover it has been found that Gd-AAZTAC17 binds with different affinities to fatted and defatted HSA as a consequence of the conformational changes that occur upon the binding of the fatty acids.^[37] The molecular docking calculations allow us to evaluate in detail the effects these conformational changes induce on the volume, polarity and solvent accessibility^[38] of the binding site I that may explain the results obtained in the relaxometric studies.

The binding energies were estimated from calculations using force field energy evaluation and thermal sampling by molecular dynamic (MD) simulations. By comparing the initial structures and the average structures computed over the last 50 ps trajectory of the MD simulation, rms coordinate deviations were calculated for all heavy (non-hydrogen) atoms within 16 Å of any ligand atoms. This yielded a rmsd value of 1.1 Å for the adduct of Gd-AAZTAC17 and fatted HSA and a value of 1.23 Å for the corresponding one with defatted HSA. The low rmsd values indicate that such simulations are expected to reproduce interactions within the binding region in a realistic fashion, that is, we can reasonably assume that no unnatural distorting forces arise in the modelling of these systems.

Energy data from the equilibration phase of the simulations were not included in the interaction energy averages. The data collection phase of the simulation was divided into two portions and the average interaction energies were calculated accordingly. The overall mean values were then determined for each of the following terms: electrostatic, van der Waals and the solvent-accessible surface area (SASA). The average differences between the bound and free-state simulations for each of the three terms are shown in Table 3. ΔU_{ele} and ΔU_{vdw} are the changes in the electrostatic

Table 3. Average differences in the ligand-surrounding interaction energies, as determined by MD simulations.

	ΔU_{ele} [kcal mol ⁻¹]	ΔU_{vdw} [kcal mol ⁻¹]	ΔSASA [Å ²]
Gd-AAZTAC17 + fatted HSA	121.234	-61.737	-676.32
Gd-AAZTAC17 + defatted HSA	158.312	-55.425	-626.32

(coulombic) and van der Waals energies, respectively, $\Delta SASA$ is the change in solvent-accessible surface area.

Molecular dynamics calculations have yielded ΔU_{vdw} average energies for the binding of Gd-AAZTAC17 to fatted HSA that are more negative than those with defatted HSA. This is in accordance with the view that Gd-AAZTAC17 can interact more deeply inside the drug site I binding cavity of fatted HSA.

If we consider the $\Delta SASA$ average for Gd-AAZTAC17, the variation in solvent-accessible surface area is greater for defatted HSA than for fatted HSA because, for defatted HSA, the molecule can insert only a small portion of the methylene tail inside the new channel arising from the rotation of Tyr 150. This results in a larger number of second-sphere water molecules in close proximity to the gadolinium chelate bound to defatted HSA than is the case with fatted HSA.

The absolute binding energies were estimated using Equation (8) (see Experimental Section), where α , β and γ were determined by fitting calculated free energies of binding to experimental results. Values of $\beta=0.001$, $\alpha=0.08$ and $\gamma=0.0026$ yielded calculated binding energies of -6.57 and -5.90 kcal mol $^{-1}$ for Gd-AAZTAC17/fatted and defatted HSA adducts, respectively, compared with experimental binding energies of -6.614 and -5.947 kcal mol $^{-1}$.

We also investigated the binding of Gd-AAZTAC17 to fatted HSA at Sudlow's site II, obtaining a binding energy of -5.02 kcal mol $^{-1}$. This value is consistent with the experimental evidence obtained from competition assays which revealed that Gd-AAZTAC17 does not bind to drug site II.

These calculations showed that upon binding of fatty acids, Tyr 150 moves and interacts with the carboxylate moiety at fatty acid site II. This structural change has a large impact on drug site I, causing a marked increase in the volume of the binding pocket.^[38]

Conversely, with defatted HSA, Gd-AAZTAC17 can fit

only half of its aliphatic tail into site I because Tyr 150 prevents it from penetrating more deeply into the binding cavity (Figure 13). The presence of Tyr 150 forces the Gd-AAZTAC17 methylene tail to bend towards the hydrophobic residues of Leu 238, Val 241 and Leu 260.

In the case of fatted HSA the movement of Tyr 150 grants access of the hydrophobic tail of Gd-AAZTAC17 to the bottom of this channel. This is a hydrophobic subchamber, delineated by Cys 245 and Cys 253 (Figure 14). The hydrophobic tail of Gd-AAZTAC17 is involved in van der Waals interactions with side-chain aliphatic carbon atoms of

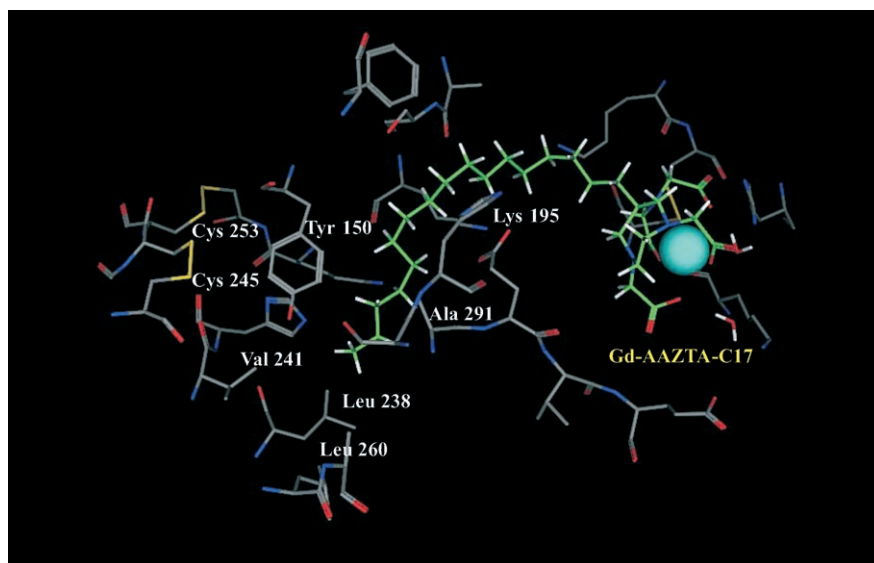


Figure 13. Graphical representation of Gd-AAZTAC17 bound to Sudlow's site I on defatted HSA determined by dynamic molecular modelling.

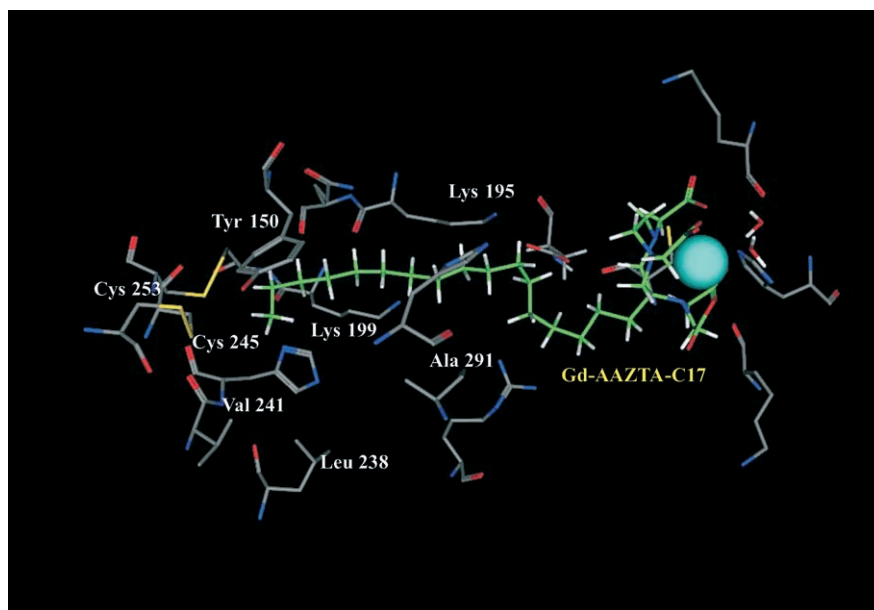


Figure 14. Graphical representation of Gd-AAZTAC17 bound to Sudlow's site I on fatted HSA determined by dynamic molecular modelling.

Lys 195, Lys 199 and Ala 291, whereas the last two methylene carbon atoms point towards Val 241.

Conclusion

The results reported in this work are relevant to the design of gadolinium-based CAs for MRI for several reasons. First of all it has been shown how the structural characteristics of the binding site may affect the relaxation enhancement. In fact it has been found that water molecules in the second coordination sphere and exchangeable protons in the proximity of the interaction site may make an important contribution to the observed relaxivity. Moreover, the imbedding of the metal chelate inside this kind of highly structured water network causes a marked increase in the water exchange rate at the paramagnetic centre. Thus it appears that two effects contribute in opposite ways to the observed relaxivity. It is likely that the use of Gd^{III} complexes characterised by a very fast exchange of the coordinated water molecule may provide a route to the attainment of very high relaxivities. In fact, it seems reasonable to expect that the lengthening caused by the embedding of such systems in the protein hydration sphere would not yield the dramatically large τ_M values that quench the attainable relaxivities. Alternatively, the design of high relaxivity agents may result in the contribution from the second coordination sphere being sacrificed to maintain a fast exchange of the coordinated water. To identify suitable binding sites in the latter systems, docking simulations may be particularly advantageous.

It has also been shown that the presence of micelles may dramatically alter the nature of the interaction of a lipophilic agent with the target protein resulting in a much smaller relaxation enhancement. This feature has to be taken into serious consideration when a lipophilic agent is administered in vivo under a highly concentrated bolus. Actually it appears likely that any self-assembled system bearing negative charges on its surface would show this type of electrostatic interaction with HSA. The formation of such a supramolecular adduct may profoundly affect the biodistribution and excretion pathways of the involved species.

Finally it has been proved that the Gd-AAZTA complex with its two coordinated water molecules is a structure of considerable interest because of its ease of synthesis and the possibility of functionalisation at the exocyclic carbon atom. Remarkably, interaction with defatted HSA provides the highest relaxivity reported so far for stable Gd^{III} chelates.

Experimental Section

Synthesis of the AAZTAC17 ligand: Ligand AAZTAC17 was synthesised following the reaction steps described in Scheme 1.

1-Nitrooctadecane (3): 3-Chloroperoxybenzoic acid (12.84 g, 74.4 mol, 85% pure) was dissolved in 1,2-dichloroethane (200 mL) in a two-necked flask equipped with a condenser and a pressure-equalising dropping funnel. Octadecylamine (**2**, 5.0 g, 18.6 mmol) in 1,2-dichloroethane (100 mL) was added dropwise to the refluxing solution. Refluxing was

continued for 30 min after the addition. Then the reaction mixture was cooled, filtered, washed with 10% aqueous Na₂CO₃ (3x100 mL) and dried (Na₂SO₄). Removal of the solvent under reduced pressure gave 1-nitrooctadecane (**3**) (3.9 g 71%). Colourless solid. M.p. 47–50°C. ¹H NMR (CDCl₃, 298 K): δ =4.37 (t, J =6.9 Hz, 2H), 2.00 (q, J =7.1 Hz, 2H), 1.41–1.19 (m, 30H), 0.87 ppm (t, J =6.6 Hz, 3H); ¹³C NMR (CDCl₃, 298 K): δ =76.0 (CH₂), 29.8 (8 CH₂), 29.7 (CH₂), 29.5 (CH₂), 29.4 (CH₂), 29.3 (CH₂), 28.9 (CH₂), 27.5 (CH₂), 26.3 (CH₂), 22.8 (CH₂), 14.2 ppm (CH₃); ESI-MS: calcd for C₁₈H₃₇NO₂: 299; found: m/z : 300 [M+H]⁺.

1,4-Dibenzyl-6-heptadecyl-6-nitro-1,4-diazepane (4): *N,N'*-Dibenzylethylenediamine diacetate (4.78 g, 13 mmol) and 1-nitrooctadecane (**3**, 3.97 g, 13 mmol) were dissolved in 1:1 toluene/methanol (100 mL) in a 500-mL round-bottomed flask. Paraformaldehyde (1.39 g, 46.5 mmol) was added portionwise to the resulting solution and the resulting suspension was refluxed. The mixture became homogeneous (dissolution of paraformaldehyde) and after 3 h at reflux, the mixture was cooled and evaporated in vacuo. The residue was recrystallised from ethanol to obtain pure **4** (4.38 g, 61%) as a colourless solid. M.p. 70–72°C (EtOH). ¹H NMR (CDCl₃, 298 K): δ =7.33–7.19 (m, 10H), 3.72 (d, J =13.0 Hz, 2H), 3.57 (d, J =13.0 Hz, 2H), 3.49 (d, J =14.2 Hz, 2H), 2.95 (d, J =14.2 Hz), 2.58 (m, 4H), 1.55 (m, 2H), 1.32–0.69 (m, 26H), 0.88 ppm (brt, 3H); ¹³C NMR (CDCl₃): δ =139.3 (C), 129.2 (CH), 128.3 (CH), 127.3 (CH), 95.2 (C), 64.1 (CH₂), 61.9 (CH₂), 58.8 (CH₂), 37.1 (CH₂), 32.0 (CH₂), 29.8 (7 CH₂), 29.7 (CH₂), 29.6 (CH₂), 29.5 (2 CH₂), 29.3 (CH₂), 23.1 (CH₂), 22.8 (CH₂), 14.2 ppm (CH₃); ESI-MS: calcd for C₃₆H₅₇N₃O₂: 563; found: m/z : 586 [M+Na]⁺, 564 [M+H]⁺.

6-Heptadecyl-1,4-diazepan-6-ylamine (5): Compound **4** (4.3 g, 7.6 mmol) was dissolved in methanol (100 mL) in a 250-mL flask. 10% Pd/C (1.0 g, moistened with 0.5 mL water) was added followed by ammonium formate (4.8 g, 76 mmol). The mixture was stirred and refluxed for 3 h. The catalyst was then removed by filtration and the filtrate evaporated in vacuo. The residue was redissolved in dichloromethane and washed with 5% aq. NaOH. The organic phase was then dried (Na₂SO₄) to give **5** (2.6 g, 91%) as a colourless wax. M.p. 66–69°C. ¹H NMR (CDCl₃, 298 K): δ =2.87 (m, 4H), 2.72 (d, J =13.5 Hz, 2H), 2.61 (d, J =13.5 Hz, 2H), 1.77 (brs, 4H), 1.32–1.20 (m, 32H), 0.87 ppm (t, J =6.7 Hz, 3H); ¹³C NMR (CDCl₃, 298 K): δ =61.0 (CH₂), 56.3 (C), 52.2 (CH₂), 40.1 (CH₂), 32.0 (CH₂), 30.5 (CH₂), 29.8 (10 CH₂), 29.4 (CH₂), 23.2 (CH₂), 22.8 (CH₂), 14.2 ppm (CH₃); ESI-MS: calcd for C₂₂H₄₇N₃: 353; found: m/z : 376 [M+Na]⁺, 354 [M+H]⁺.

[6-Bis(tert-butoxycarbonylmethyl)amino-4-tert-butoxycarbonylmethyl-6-heptadecyl-1,4-diazepan-1-yl]acetic acid tert-butyl ester (6): The amine **5** (1.65 g 4.7 mmol) was dissolved in acetonitrile (15 mL) in a 50 mL round-bottomed flask and K₂CO₃ (5.16 g, 37 mmol) was added. *tert*-Butyl bromoacetate (4.55 g, 23.4 mmol) was slowly added dropwise to the stirred heterogeneous mixture while maintaining the temperature at <10°C (ice bath). After the addition the mixture was heated at 60°C with stirring until TLC showed complete conversion. The precipitate was filtered and washed with dichloromethane; the filtrate and the washings were combined and evaporated in vacuo to give the crude product. The semisolid residue was purified by silica gel chromatography (petroleum ether/ethyl acetate 9.3:0.7), giving pure **6** as a pale yellow oil (1.35 g, 36%). ¹H NMR (CDCl₃, 298 K): δ =3.63 (s, 4H), 3.22 (s, 4H), 2.99 (d, J =14.0 Hz, 2H), 2.75 (m, 4H), 2.64 (d, J =14.0 Hz, 2H), 1.44 (s, 18H), 1.43 (s, 18H), 1.24 (m, 32H), 0.85 ppm (brt, 2H); ¹³C NMR (CDCl₃, 298 K): δ =173.0 (C), 170.9 (C), 80.7 (C), 80.2 (C), 65.4 (CH₂), 63.2 (C), 62.6 (CH₂), 59.4 (CH₂), 52.0 (CH₂), 37.7 (CH₂), 32.0 (CH₂), 30.6 (CH₂), 29.9 (CH₂), 29.8 (9 CH₂), 29.4 (CH₂), 28.3 (CH₃), 28.2 (CH₃), 22.8 (CH₂), 22.1 (CH₂), 14.2 ppm (CH₃); ESI-MS: calcd for C₄₆H₈₇N₃O₈: 809; found: m/z : 832 [M+Na]⁺, 810 [M+H]⁺.

[6-Bis(carboxymethyl)amino-4-carboxymethyl-6-heptadecyl-1,4-diazepan-1-yl]acetic acid (1): The ester **6** (1.354 g 1.7 mmol) was dissolved in trifluoroacetic acid (20 mL) in a 50-mL round-bottomed flask and stirred at room temperature overnight. The solution was then evaporated in vacuo and the residue was redissolved in methanol (2 mL). The product precipitated from solution on addition of excess diethyl ether, was isolated by centrifugation, washed thoroughly with diethyl ether and dried in vacuo, giving pure **1** (795 mg, 81%) as an amorphous white solid. M.p. 185–

187 °C (decomp). ^1H NMR (CD_3OD , 298 K): δ = 3.85 (d, J = 17.8 Hz, 2H), 3.80 (d, J = 17.8 Hz, 2H), 3.71 (s, 4H), 3.35 (d, J = 14.3 Hz, 2H), 3.34 (s, 4H), 3.24 (d, J = 14.3 Hz, 2H), 1.39 (m, 2H), 1.28 (m, 30H), 0.89 ppm (t, J = 6.7 Hz, 3H); ^{13}C NMR (CD_3OD , 298 K): δ = 175.8 (C), 170.0 (C), 62.5 (C), 60.5 (CH_2), 57.8 (CH_2), 53.1 (CH_2), 50.3 (CH_2), 35.5 (CH_2), 31.8 (CH_2), 30.0 (CH_2), 29.5 (9 CH_2), 29.3 (CH_2), 29.2 (CH_2), 23.1 (CH_2), 22.5 (CH_2), 13.2 ppm (CH_3); ESI-MS: calcd for $\text{C}_{30}\text{H}_{55}\text{N}_5\text{O}_8$: 585; found: m/z : 608 $[\text{M} + \text{Na}]^+$, 586 $[\text{M} + \text{H}]^+$.

Complexation of AAZTAC17 with Gd^{III} : The Gd^{III} complex was readily synthesised by adding stoichiometric amounts of the ligand and GdCl_3 at room temperature. The excess free gadolinium was removed by filtering the basic solution with 0.2 μm syringe filters. Orange Xylenol UV spectrophotometry was used to check for the absence of free Gd^{III} ions.^[45]

Water proton relaxivity measurements: The longitudinal water proton relaxation rates were measured by using a Stellar Spinmaster (Mede, Pavia, Italy) spectrometer operating at 0.47 T by the standard inversion-recovery technique (16 experiments, 2 scans). A typical 90° pulse width was 3.5 μs and the reproducibility of the T_1 data was $\pm 0.5\%$. The temperature was controlled with a Stellar VTC-91 air-flow heater equipped with a copper/constantan thermocouple (uncertainty ± 0.1 °C). The proton $1/T_1$ NMRD profiles were measured over a continuum of magnetic field strength from 0.00024 to 0.47 T (corresponding to a 0.01–20 MHz proton Larmor frequency) on a Stellar field-cycling relaxometer. The relaxometer operates under complete computer control with an absolute uncertainty in $1/T_1$ of $\pm 1\%$. Data points from 0.47 (20 MHz) to 1.7 T (70 MHz) were collected on a Stellar Spinmaster spectrometer operating at variable fields.

^{17}O measurements: Variable-temperature ^{17}O NMR measurements were recorded with a JEOL EX-90 spectrometer equipped with a 5 mm probe using a D_2O external lock. Experimental settings were as follows: spectral width 10000 Hz, 90° pulse width (7 μs), acquisition time 10 ms, 1000 scans and no sample spinning. Solutions containing 2.6% of the ^{17}O isotope (Yeda, Israel) were used. The observed transverse relaxation rates ($R_{2\text{obs}}^0$) were calculated from the signal width at half-height ($\Delta\nu/2$): $R_{2\text{obs}}^0 = \pi\Delta\nu/2$

Light scattering measurements: Dynamic light scattering measurements, made to determine the size of the micellar system, were performed on a Malvern Zetasizer Nano ZS apparatus. The size range over which the instrument can operate is 0.6 nm–6 μm . A laser was used as the light source to illuminate the sample particles within a cell. A detector, positioned at 173°, was used to measure the intensity of the light scattered by the particles of the sample. An attenuator was used to reduce the intensity of the laser and hence reduce the intensity of the scattering which has to be within a specific range for the detector to successfully measure it. The position of the attenuator was determined automatically by the Zetasizer during the measurement process. The scattering intensity detected was passed to a digital signal processing board called a correlator. The correlator compares the scattering intensity at successive time intervals to derive the rate at which the intensity varies. This correlator information was then passed to a computer where the specialist Zetasizer software analyses the data and derives size information.

Molecular weight measurements of the Gd-AAZTAC17 micellar system were managed using the molecular weight function in the DTS software of the Zetasizer Nano system, which compiles the static intensity measurements, generates a standard Debye plot and then calculates the molecular weight and second virial coefficient. Molecular weight measurements were performed in water using a dn/dc value of 0.12 mL g^{-1} .^[27,28] Different sample concentrations were prepared by diluting a high concentration stock solution and filtering through 100 nm Anotop filters prior to measurement. Both the toluene reference and solvent were double-filtered through 20 nm Anotop filters prior to measurement.

Computational methods: All computer modelling procedures were carried out using the Moe program (Chemical Computing Group, Inc., MOE 2004.03 (www-chemcomp.com)). The high-resolution three-dimensional coordinates of human serum albumin (HSA), fat-free and complexed with stearic acid, were obtained from the Protein Data Bank (PDB code 2bcx and 1E7I). The structures were prepared for docking calculations by adding hydrogen atoms and completing missing atoms.

Minimisation was achieved by a multistep procedure, first fixing all heavy atoms and relaxing the positions of the added hydrogen atoms, then through geometry optimisation of the hydrogen atoms and side-chains while keeping the backbone atoms fixed, and finally through full geometry optimisation without constraints until convergence was less than 0.01 $\text{kcal mol}^{-1} \text{Å}^{-1}$ with steepest-descent and conjugate gradient methods.

The ligand structure of Gd-AAZTA was constructed starting from the crystal structure of the AAZTA-like cycle obtained from the CSD (RULLEP code) with the Moe-Builder module and optimised by ab initio methods. Full geometry optimisation was performed at the RHF level with Gaussian 98^[46] using an effective core potential (ECP) that includes 4f electrons in the core (1s–4d,4f)^[47] and an optimised valence basis set for the metal and 3-21G basis sets for ligand atoms.^[48] The methylene tail was added with the Moe-Builder module and minimised keeping the AAZTA cycle fixed.

Partial charges were calculated by the Mulliken method implemented in Gaussian 98 at the RHF level of theory using the 6-31G* basis set for ligand atoms and the ECP for the gadolinium atom with a pseudopotential according to Dolg and Stoll.^[48] The calculated charges were averaged over all atoms of the same type, with the metal ion maintaining a +3 atomic charge^[49] and the total charge was then corrected by distributing the excess charge onto donor atoms.

For all the calculations a modification of the Amber99 force field^[50] was used with in-house parametrisation to treat gadolinium complexes within the framework of the ionic method.^[51] The σ and ϵ van der Waals parameters for Gd^{3+} were chosen to reproduce the experimental (crystallographic) coordination structures of the Gd-DOTA and Gd-DTPA complexes (CSD code: JOPJIH and HEQBUA, respectively). This was achieved by energy minimisation and by systematically changing the value of σ and ϵ between each minimisation in order to reproduce the crystallographic geometry (lower RMSD values).^[52]

The method was evaluated using known structures, obtaining the best fit to crystal structures with $\sigma = 1.8 \text{ Å}$ and $\epsilon = 0.1$, giving rms deviations of 0.32 Å for Gd-DOTA and 0.31 Å for Gd-DTPA.

The starting positions for the docking procedure were obtained by modifying the ligand positions, orientations and conformations to optimise binding geometry while filling the available space in the HSA drug site I. The docking procedure was performed using the Moe-Dock module with Tabu Search with 10 runs, 1000 steps per run. The ligand was kept partially flexible.

The best solution from the docking calculations was submitted to molecular dynamics simulations of the bound and unbound ligand, the solvating ligand and protein–ligand complexes with 20 Å spheres of TIP3P water molecules. For the simulations of the ligand bound to the protein, residues within 20 Å of the binding site were included; the outer residues were kept frozen. The simulation of the free state was carried out in a sphere of equal size filled with water molecules and with the ligand at the centre.

In both simulations the water molecules were restrained to prevent vapourisation using a half-harmonic restraint 20 Å from the ligand atoms with a force constant of 20 $\text{kcal mol}^{-1} \text{Å}^{-2}$.

To have the same net charge in the bound and free states to avoid Born-type corrections,^[53] excess charge on the protein must be removed. To fulfil this requirement, charged residues far from the ligand and near the boundary of the simulation sphere were neutralised.^[54]

Molecular dynamics simulations were performed with the NVT ensemble keeping the temperature constant at 30 °C, as in the binding experiment. After minimisation of the water sphere until a rms gradient of 0.01 $\text{kcal mol}^{-1} \text{Å}$ was obtained, the temperature was increased to 300 K, followed by 20 ps of equilibration of water molecules keeping the ligand fixed, then 20 ps of equilibration of the entire system. Data were collected during the next 100 ps of the simulations.

The free energies of binding were estimated using a recently reported method proposed and successfully tested on different endothiapepsin inhibitor complexes by Aqvist et al.^[55] This method is based on standard thermodynamic cycles and on linear approximation of polar and non-

polar free energy contributions from the corresponding electrostatic and van der Waals energy averages. The free energy of binding ΔG_b of a ligand is approximated by Equation (8), where the ΔU energies are, respectively, the electrostatic and van der Waals energy differences between the ligand in the solvated protein (bound state) and the ligand in the sphere of the water molecules (free state).

$$\Delta G_b = \beta < \Delta U_{\text{ele}} > + \alpha < \Delta U_{\text{vdw}} > + \gamma < \Delta \text{SASA} > \quad (8)$$

Furthermore, the binding free energy is not determined by a single conformation from the docking procedure, but indeed by a thermal average. Therefore this approach tries to capture conformational fluctuations that are important for the binding energy.

Interaction energies for the ligand in the binding pocket of the solvated protein and in the aqueous environment were extracted using a 16 Å cut-off value.

Solvent accessible surface area calculations were carried out after the simulations on coordinates recorded every 0.5 ps of the sampling phase. Average energies and SASA differences were fitted to the experimental ΔG binding values to obtain linear response parameters α , β and γ according to Equation (8). This procedure was performed with a genetic algorithm. Experimental ΔG values were calculated from K_A values reported in Table 2 ($\Delta G = -RT \ln K_A$).

Acknowledgements

Support from Bracco Imaging Spa, PRIN 2005, Noe-EMIL and DiMI is gratefully acknowledged. This work was carried out within the framework of EU-Cost D18 Action.

- [1] R. B. Lauffer, *Chem. Rev.* **1987**, *87*, 901–927.
- [2] A. E. Merbach, E. Toth, *The Chemistry of Contrast Agents in Medical Magnetic Resonance Imaging*, Wiley, Chichester, **2001**.
- [3] S. Aime, M. Botta, M. Fasano, E. Terreno, *Chem. Soc. Rev.* **1998**, *27*, 19–29.
- [4] P. Caravan, J. J. Ellison, T. J. McMurry, R. B. Lauffer, *Chem. Rev.* **1999**, *99*, 2293–2352.
- [5] H. J. Weinmann, A. Mühler, B. Radüchel in *Biomedical Magnetic Resonance Imaging and Spectroscopy* (Ed.: I. R. Young), Wiley, Chichester, **2000**, p. 705.
- [6] L. Banci, I. Bertini, C. Luchinat, *Nuclear and Electronic Relaxation*, VCH, Weinheim, **1991**.
- [7] S. Aime, A. Barge, E. Gianolio, S. Geninatti Crich, W. Dastrù, F. Uggeri in *Metallotherapeutic drugs & metal based Diagnostic Agents; The use of Metals in Medicine*, (Eds.: M. Gielen, E. R. T. Tiekink), Wiley, **2005**, p.541.
- [8] S. Aime, M. Botta, M. Fasano, E. Terreno, *Protein-bound metal chelates in The chemistry of contrast agents in medical Magnetic Resonance Imaging*. (Eds.: A. E. Merbach, E. Toth), Wiley, Chichester, **2001**, p. 193.
- [9] M. H. Ou, C. H. Tu, S. C. Tsai, W. T. Lee, G. C. Lin, Y. M. Wang, *Inorg. Chem.* **2006**, *45*, 244–254.
- [10] S. Aime, M. Chiaussa, G. Digilio, E. Gianolio, E. Terreno, *J. Biol. Inorg. Chem.* **1999**, *4*, 766–774.
- [11] S. Aime, E. Gianolio, D. Longo, R. Pagliarin, C. Lovazzano, M. Sisti, *ChemBioChem* **2005**, *6*, 818.
- [12] F. A. Dunand, A. Borel, A. E. Merbach, *J. Am. Chem. Soc.* **2002**, *124*, 710–716.
- [13] S. Aime, E. Gianolio, E. Terreno, G. B. Giovenzana, R. Pagliarin, M. Sisti, G. Palmisano, M. Botta, M. Lowe, D. Parker, *J. Biol. Inorg. Chem.* **2000**, *5*, 488–497.
- [14] S. Aime, M. Botta, S. Geninatti Crich, G. B. Giovenzana, R. Pagliarin, M. Sisti, E. Terreno, *Magn. Reson. Chem.* **1998**, *36*, 200–208.
- [15] S. Aime, M. Botta, S. Geninatti Crich, G. B. Giovenzana, G. Jommi, R. Pagliarin, M. Sisti, *Inorg. Chem.* **1997**, *36*, 2992–3000.
- [16] S. Aime, M. Botta, S. Geninatti Crich, G. B. Giovenzana, G. Jommi, R. Pagliarin, M. Sisti, *J. Chem. Soc., Chem. Commun.* **1995**, 1885–1886.
- [17] S. Aime, E. Gianolio, D. Corpillo, C. Cavallotti, G. Palmisano, M. Sisti, G. B. Giovenzana, *Helv. Chim. Acta* **2003**, *86*, 615–632.
- [18] J. Xu, S. J. Franklin, Jr., D. W. Whisenhunt, K. N. Raymond, *J. Am. Chem. Soc.* **1995**, *117*, 7245–7246.
- [19] S. Hajela, M. Botta, S. Giraud, J. Xu, K. N. Raymond, S. Aime, *J. Am. Chem. Soc.* **2000**, *122*, 11228–11229.
- [20] D. M. J. Doble, M. Botta, J. Wang, S. Aime, A. Barge, K. N. Raymond, *J. Am. Chem. Soc.* **2001**, *123*, 10758–10759.
- [21] S. Aime, L. Calabi, C. Cavallotti, E. Gianolio, G. B. Giovenzana, P. Losi, A. Maiocchi, G. Palmisano, M. Sisti, *Inorg. Chem.* **2004**, *43*, 7588–7590.
- [22] S. H. Koenig, R. D. Brown, *Prog. Nucl. Magn. Reson. Spectrosc.* **1990**, *26*, 487–567.
- [23] D. H. Powell, O. M. Ni Dhubhghaill, D. Pubanz, L. Helm, Y. S. Lebedev, V. Schlaepfer, A. E. Merbach, *J. Am. Chem. Soc.* **1996**, *118*, 9333–9346.
- [24] S. Aime, M. Botta, M. Fasano, E. Terreno, *Acc. Chem. Res.* **1999**, *32*, 941–949.
- [25] G. M. Nicolle, E. Toth, K. P. Eisenwiener, H. R. Macke, A. E. Merbach, *J. Biol. Inorg. Chem.* **2002**, *7*, 757–769.
- [26] S. Laus, A. Sour, R. Ruloff, E. Toth, A. E. Merbach, *Chem. Eur. J.* **2005**, *11*, 3064–3076.
- [27] G. M. Nicolle, L. Helm, A. E. Merbach, *Magn. Reson. Chem.* **2003**, *41*, 794–799.
- [28] H. G. Thomas, A. Lomakin, D. Blankshtein, G. B. Benedek, *Langmuir* **1997**, *13*, 209–218.
- [29] V. Schadler, C. Nardin, U. Wiesner, E. Mendes, *J. Phys. Chem. B* **2000**, *104*, 5049–5052.
- [30] P. Debye, *J. Appl. Phys.* **1944**, *15*, 338–343.
- [31] P. J. Wyatt, *Anal. Chim. Acta* **1993**, *272*, 1–40.
- [32] K. Mattison, M. Kaszuba, *American Biotechnology Laboratory*, June **2003**.
- [33] U. Kragh-Hansen, *Dan. Med. Bull.* **1990**, *37*, 57–84.
- [34] D. C. Carter, J. X. Ho, *Adv. Protein Chem.* **1994**, *47*, 152–203.
- [35] T. J. Peters, *All about Albumin: biochemistry, genetics and medical applications*, Academic Press, San Diego, **1996**.
- [36] S. Curry, P. Brick, N. P. Franks, *Biochim. Biophys. Acta* **1999**, *1441*, 131–140.
- [37] S. Curry, H. Mandelkov, P. Brick, N. Franks, *Nat. Struct. Biol.* **1998**, *5*, 827–835.
- [38] J. Ghuman, P. A. Zunszain, I. Petitpas, A. A. Bhattacharya, M. Ottagiri, S. Curry, *J. Mol. Biol.* **2005**, *353*, 38–52.
- [39] J. B. Livramento, C. Weidensteiner, M. I. M. Prata, P. R. Allegrini, C. F. G. C. Geraldes, L. Helm, R. Kneuer, A. E. Merbach, A. C. Santos, P. Schmidt, E. Toth, *Contrast Media Mol. Imaging* **2006**, *1*, 30–39.
- [40] X. M. He, D. C. Carter, *Nature* **1992**, *358*, 209–215.
- [41] R. Reed, *J. Biol. Chem.* **1977**, *252*, 7483–7487.
- [42] H. Vorum, B. Honorè, *J. Pharm. Pharmacol.* **1996**, *48*, 870–875.
- [43] S. Sugio, A. Kashima, S. Mochizuki, M. Noda, K. Kobayashi, *Protein Eng.* **1999**, *12*, 439–446.
- [44] S. Aime, M. Botta, F. Fedeli, E. Gianolio, E. Terreno, P. L. Anelli, *Chem. Eur. J.* **2001**, *7*, 5261–5269.
- [45] A. Barge, G. Cravotto, E. Gianolio, F. Fedeli, *Contrast Media Mol. Imaging* **2006**, *1*, 184–188.
- [46] Gaussian 98, Revision A.11, M. J. Frisch, G. W. Trucks, H. B. Schlegel, G. E. Scuseria, M. A. Robb, J. R. Cheeseman, V. G. Zakrzewski, J. A. Montgomery, Jr., R. E. Stratmann, J. C. Burant, S. Dapprich, J. M. Millam, A. D. Daniels, K. N. Kudin, M. C. Strain, O. Farkas, J. Tomasi, V. Barone, M. Cossi, R. Cammi, B. Mennucci, C. Pomelli, C. Adamo, S. Clifford, J. Ochterski, G. A. Petersson, P. Y. Ayala, Q. Cui, K. Morokuma, P. Salvador, J. J. Dannenberg, D. K. Malick, A. D. Rabuck, K. Raghavachari, J. B. Foresman, J. Cioslowski, J. V. Ortiz, A. G. Baboul, B. B. Stefanov, G. Liu, A. Liashenko, P. Piskorz,

- I. Komaromi, R. Gomperts, R. L. Martin, D. J. Fox, T. Keith, M. A. Al-Laham, C. Y. Peng, A. Nanayakkara, M. Challacombe, P. M. W. Gill, B. Johnson, W. Chen, M. W. Wong, J. L. Andres, C. Gonzalez, M. Head-Gordon, E. S. Replogle, J. A. Pople, Gaussian, Inc., Pittsburgh, PA, **2001**.
- [47] U. Cosentino, G. Moro, D. Pitea, A. Villa, P. C. Fantucci, A. Maiocchi, F. Uggeri, *J. Phys. Chem. A* **1998**, *102*, 4606–4614.
- [48] M. Dolg, H. Stoll, *Theor. Chim. Acta* **1989**, *75*, 173–179.
- [49] F. Yerly, K. I. Hardcastle, L. Helm, S. Aime, M. Botta, A. E. Merbach, *Chem. Eur. J.* **2002**, *8*, 1031–1039.
- [50] J. W. Ponder, D. A. Case, *Adv. Protein Chem.* **2003**, *66*, 27–35.
- [51] B. P. Hay, *Coord. Chem. Rev.* **1993**, *126*, 177–236.
- [52] R. Fossheim, S. G. Dahl, *Acta Chem. Scand.* **1990**, *44*, 698–706.
- [53] J. Aqvist, C. Medina, J. E. Samuelsson, *Protein Eng.* **1994**, *7*, 385–391.
- [54] J. Aqvist, *J. Comput. Chem.* **1996**, *17*, 1587–1597.

Received: September 5, 2006
Published online: April 3, 2007